iScience

CellPress
OPEN ACCESS

Article

Polymerizable metal-organic frameworks for the preparation of mixed matrix membranes with enhanced interfacial compatibility

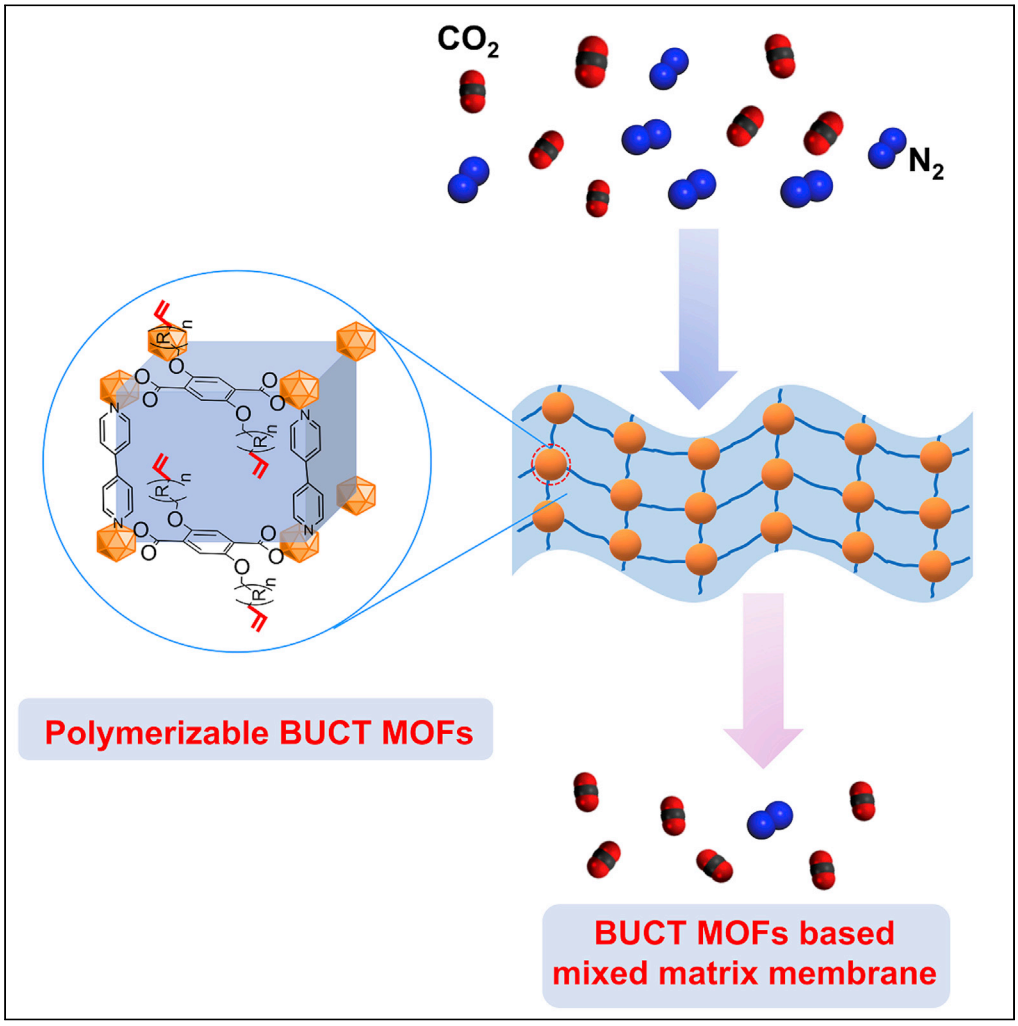

Ziman Chen, Dong Yan, Liang Ma, ..., Frantisek Svec, Yongqin Lv, Tianwei Tan

lvyq@mail.buct.edu.cn

Highlights

A new class of vinyl-containing MOFs was constructed for the separation of CO_2 and N_2.

The structure of BUCT MOFs were analyzed by single-crystal X-ray crystallography.

The C=C double bonds of BUCT MOFs can serve as polymerizable groups with high activity.

BUCT-2 based MMM exhibited a superior CO_2/N_2 selectivity of 41.6.

Chen et al., iScience 24, 102560
June 25, 2021
https://doi.org/10.1016/j.isci.2021.102560

iScience

CellPress
OPEN ACCESS

Article

Polymerizable metal-organic frameworks for the preparation of mixed matrix membranes with enhanced interfacial compatibility

Ziman Chen,[1,2] Dong Yan,[1,2] Liang Ma,[1,2] Yahui Zhang,[1] Jingyan Zhang,[2] Hui Li,[2] Rebecca Khoo,[3] Jian Zhang,[3] Frantisek Svec,[2,4] Yongqin Lv,[1,5,*] and Tianwei Tan[1]

SUMMARY

The preparation of flawless and defect-free mixed matrix membranes (MMMs) comprising metal-organic framework (MOF) and polymer is often difficult owing to the poor MOF/polymer interface compatibility. Herein, we present the synthesis of an important family of pillared-layered MOFs with polymerizable moieties based on the parent structure $[Zn_2L_2P]_n$ [L = vinyl containing benzenedicarboxylic acid linkers; P = 4,4′-bipyridine (bipy)]. The crystalline structures of polymerizable MOFs were analyzed using single-crystal X-ray crystallography. The presence of reactive double bonds in MOFs was verified by the successful thiol-ene click reaction with sulfhydryl compounds. The subsequent copolymerization of polymerizable MOFs with organic monomers produced mixed matrix membranes with enhanced MOF/polymer interfacial adhesion that enabled good separation efficiency of CO_2 from flue gas. This strategy provides a stimulating platform to the preparation of highly efficient MMMs that are capable of mitigating energy consumption and environment issues.

INTRODUCTION

The anthropogenic carbon dioxide (CO_2) emissions from fossil fuels burning have become the leading cause of greenhouse effect and global warming. Advanced methods and technologies are highly desirable to alleviate the rising level of CO_2 in the atmosphere for sustainable development (D'Alessandro et al., 2010; Wang et al., 2016; Yu et al., 2017). Over the past few decades, membrane-based separation has attracted enormous attention as a promising strategy to remove CO_2 from flue gas or natural gas. Compared with the conventional separation technologies, membranes are relatively simple and low cost, easily scalable, and less energy intensive (Baker and Low, 2014; Bernardo et al., 2009; Brunetti et al., 2010; Javaid, 2005; Prasetya et al., 2020). Polymer membranes possessing good thermal and mechanical properties have been widely used for CO_2 separation. However, they suffer from the substantial obstacles of the well-known "trade-off" between permeability and selectivity that limits their separation performances (Park et al., 2017). Inorganic membranes generally produce good performances but are more expensive and difficult to prepare. In this respect, mixed matrix membranes (MMMs) that integrate the low cost and easy production of polymer matrix with the selectivity of inorganic fillers may fulfill the requirement of feasible separation process (Goh et al., 2011; Rezakazemi et al., 2014).

As an emerging class of highly porous materials, metal-organic frameworks (MOFs) with three-dimensional lattice are formed via the coordination of inorganic metal ions and organic linkers (Furukawa et al., 2013; Li et al., 1999; Zhou and Kitagawa, 2014). Owing to their large surface area and porosity, well-defined chemistry, and structural diversity, MOFs have been extensively explored as fillers in the design of MMMs (Dechnik et al., 2017; Deng et al., 2021; Denny et al., 2016; Guo et al., 2019, 2021; Lin et al., 2018; Ma et al., 2019a; Seoane et al., 2015). The MOF-based MMMs are typically prepared by admixing the preformed MOF nanoparticles in the polymer solution to obtain the final casting mixture. However, preparing robust and defect-free MMMs still remains a challenge owing to the poor compatibility between MOF and polymer matrices, as well as the undesired MOF particle sedimentation (Dong et al., 2013; Lin et al., 2018; Moore and Koros, 2005). Some successful strategies have been developed to construct MOF-based MMMs by chemical modification of MOFs or polymer matrices (Elsaidi et al., 2020; Tien-Binh et al., 2015; Venna et al., 2015; Wang et al., 2018), introduction of MOF/polymer interface layers (Bastani et al., 2013; Feijani et al.,

[1]Beijing Key Laboratory of Bioprocess, College of Life Science and Technology, Beijing University of Chemical Technology, No 15 North Third Ring East Road, Chaoyang District, Beijing 100029, China

[2]Beijing Advanced Innovation Center for Soft Matter Science and Engineering, College of Life Science and Technology, Beijing University of Chemical Technology, No 15 North Third Ring East Road, Chaoyang District, Beijing 100029, China

[3]Molecular Foundry, Lawrence Berkeley National Laboratory, Berkeley, CA 94720, United States

[4]Department of Analytical Chemistry Faculty of Pharmacy, Charles University, 500 05 Hradec Králové, Czech Republic

[5]Lead contact

*Correspondence: lvyq@mail.buct.edu.cn

https://doi.org/10.1016/j.isci.2021.102560

2015), and *in situ* MOF growth by direct admixing MOF precursors in the monomer/polymer solution (Kertik et al., 2017; Ma et al., 2019b; Shahid et al., 2015).

Integrating MOFs with polymer components via covalent bonding is one of the promising approaches. MOFs with polymerizable moieties are excellent candidates for the production of flawless composites via its copolymerization with organic monomers (Chang et al., 2020; Hou et al., 2016; Venna et al., 2015; Wang et al., 2018; Yoo et al., 2020). For instance, the state-of-the-art methods for the preparation of MOFs with polymerizable double bonds typically rely on postsynthetic modification (Albalad et al., 2018; Cohen, 2012, 2017; Garzón-Tovar et al., 2017; Morris et al., 2008; Yin et al., 2019) of presynthesized MOF particles containing amine groups to introduce methacrylate moieties on the MOF surface (Jiang et al., 2016; Molavi et al., 2018; Zhang et al., 2015). Despite their advances, most of the current methods still involve tedious procedures requiring long reaction times and high temperature. More importantly, the yields of double bonds are generally low as the modification reaction is limited by the diffusion of reagents to the active sites of solid MOFs.

Herein, we propose the preparation of a new type of pillared-layered MOFs (named as BUCT, Beijing University of Chemical Technology) that contain polymerizable moieties using the "bottom-up" strategy. The organic linkers containing vinyl groups are first synthesized and then coordinated with metal ions to produce the polymerizable MOFs. This strategy enables the formation of MOFs with highly accessible vinyl functionalities. The structure of polymerizable MOF was analyzed using single-crystal X-ray crystallography, while their gas adsorption properties were calculated using density functional theory (DFT). The pillared-layered structure and surface chemistry of MOFs afforded high affinity and selectivity toward CO_2 over N_2. The reactivity of these MOFs was demonstrated by copolymerization with vinyl- and thiol-containing functional monomers. The resulting MOF-polymer MMMs which were provided by copolymerizing vinyl-containing MOFs with vinyl monomers have reduced stand-alone defect and exhibit excellent performances in the separation of CO_2 and N_2 (Scheme 1).

RESULTS AND DISCUSSION

Construction and characterizations of vinyl-containing BUCT MOFs

Isoreticular MOFs with pillared-layered frameworks $[M_2L_2P]_n$ (M = Zn^{2+}, Cu^{2+}; L = linear dicarboxylate linker; P = neutral pillar) have been widely studied owing to their guest and temperature-dependent structural changes and breathing behavior (Henke and Fischer, 2011; Henke et al., 2012). Inspired by these studies, we report here the preparation of two new polymerizable Zn-containing pillared-layered MOFs $[Zn_2L_2P]_n$ [L = vinyl containing terephthalic acid; P = 4,4′-bipyridine (bipy)] that we named as BUCT-1 and BUCT-2. They are formed via the coordination of Zn_4O nodes with 4,4′-bipyridine and vinyl-containing organic linkers (Scheme S1). Two organic linkers containing polymerizable double bonds, 2,5-bis((4-vinylbenzyl)oxy)-1,4-benzenedicarboxylic acid (linker 1) and 2,5-bis(oct-7-en-1-yloxy)-1,4-benzenedicarboxylic acid (linker 2), were synthesized at first. ^1H and ^{13}C nuclear magnetic resonance (NMR) spectra in Figures S1–S6 verified the successful synthesis of the linkers containing double bonds. The electrospray ionisation mass spectrometry (ESI-MS) spectra showed the corresponding peaks at m/z 429.1 for linker 1 and 417.2 for linker 2 (Figures S7 and S8). The polymerizable double bonds of linkers 2 were coupled to the terephthalic acid core through flexible alkyl chains that might increase the conformational flexibility of side chains, making them more suitable for the copolymerization with other monomers.

Solvothermal reactions of $Zn(NO_3)_2 \cdot 6H_2O$ with 4,4′-bipyridine and vinyl-containing linkers (linkers 1 and 2) were carried out at 85°C in the mixture of *N*,*N*′-dimethylformamide (DMF) and ethanol for 48 h, resulting in light yellow MOF crystals (BUCT-1 and BUCT-2). The MOFs were repeatedly washed with fresh DMF and ethanol and then activated via immersing the crystals in CH_2Cl_2 for 8 h followed by drying under vacuum at 120°C overnight. This treatment produced guest-free MOF-crystals with estimated formulas Zn_2(linker)$_2$(bipy) [BUCT-1, $Zn_2(C_{26}H_{22}O_6)_2(C_{10}H_8N_2)$; BUCT-2, $Zn_2(C_{24}H_{34}O_6)_2(C_{10}H_8N_2)$] as determined by energy-dispersive X-ray spectroscopy elemental analysis (Figures S9 and S10 and Tables S1 and S2) and single-crystal X-ray diffraction. Powder X-ray diffraction (PXRD) and thermal gravimetric analysis (TGA) were used to verify the phase purity of MOFs. The PXRD patterns of guest-free phase BUCT MOFs in Figure 1A confirmed a good crystallinity and underlying topology. The two BUCT MOFs featured similar prominent peaks indicating their analogous crystallinity. The characteristic peaks in the PXRD spectra matched those of the simulated BUCT patterns and as-synthesized MOF-508. The residual weight of zinc oxide determined from the TGA traces in Figure S11 was 15.2 wt% for BUCT-1 and 14.3 wt% for BUCT-2 (Table S3),

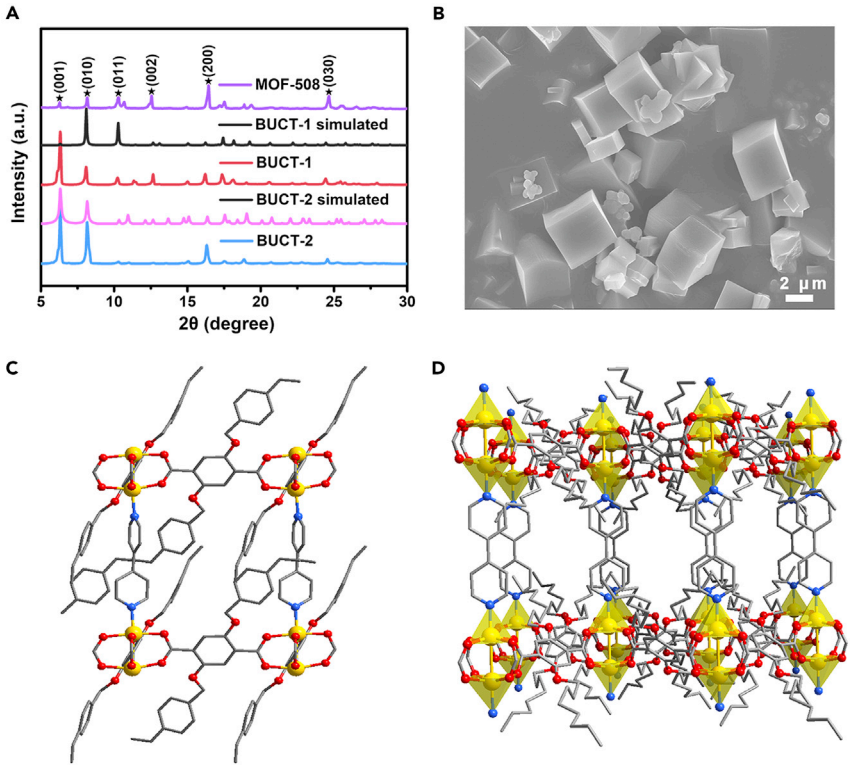

Figure 1. The structural and morphology characterizations of BUCT MOFs

Powder XRD patterns of BUCT-1, BUCT-2, and MOF-508 (A); The SEM image of BUCT-1 (B); Single-crystal structure of BUCT-1 (C) and BUCT-2 (D) (hydrogen atoms and counter anions are omitted for clarity, gray: C; red: O; yellow: Zn(II); light blue: N).

which were consistent with the calculated Zn content value of 11.4 wt% and 11.7 wt%, respectively. Scanning electron microscopy (SEM) images in Figures 1B and S12 revealed cubic and cuboid morphologies for BUCT-1 and BUCT-2.

Crystal structure and gas adsorption behavior of BUCT MOFs

The crystal structures of BUCT-1 and BUCT-2 were determined by single-crystal X-ray diffraction analysis. Single yellow cubic- and needle-shaped crystals of BUCT-1 and BUCT-2 were obtained, respectively, via the solvothermal method. The two MOFs displayed similar structural connectivity and selected metric parameters (Tables S4 and S5). As displayed in Figures 1C and 1D, the two BUCT MOFs contained a "paddle-wheel" binuclear zinc carboxylate unit $[Zn_2(COO)_4]$ in the corner of the cubical architecture, which were bridged by the vinyl-containing carboxylate-based ligands. The distorted 2-dimensional square grids were pillared by 4,4′-bipyridine molecules through coordination between the nitrogen atoms and the axial sites of the $[Zn_2(COO)_4]$ paddle wheels, giving rise to a structural integrity 3-dimensional framework with an elongated cubic lattice. The sorption isotherms of N_2 and CO_2 were recorded at 273 K to evaluate the adsorption behavior of BUCT MOFs (Figure 2). Interestingly, these two MOFs show almost no uptake of N_2 even at 77 K (Figure S13). The slight capacity of 1 cm^3 (STP)/g at 1 bar can be ascribed to the adsorption on MOF outer surface instead of within the pores (Henke and Fischer, 2011). By contrast, BUCT-1 and BUCT-2 exhibited high uptake capacities for CO_2 at 273 K, which were 15- and 20-fold higher than that found for N_2. The CO_2 adsorption/desorption isotherms corresponded to type-I isotherm. This could be ascribing to the polar molecules such as CO_2 can easily penetrate through the void space owing to the polar nature of the ether chains, while the N_2 molecules cannot (Henke et al., 2010).

The first principle calculations were carried out to better evaluate the nanopore structures and gas adsorption properties of BUCT MOFs [Figures 2C–2E)]. From the top view of atomic structure of BUCT-1, a 1D nanopore structure with diameter of 6.3 Å along the z axis could be clearly observed. The adsorption

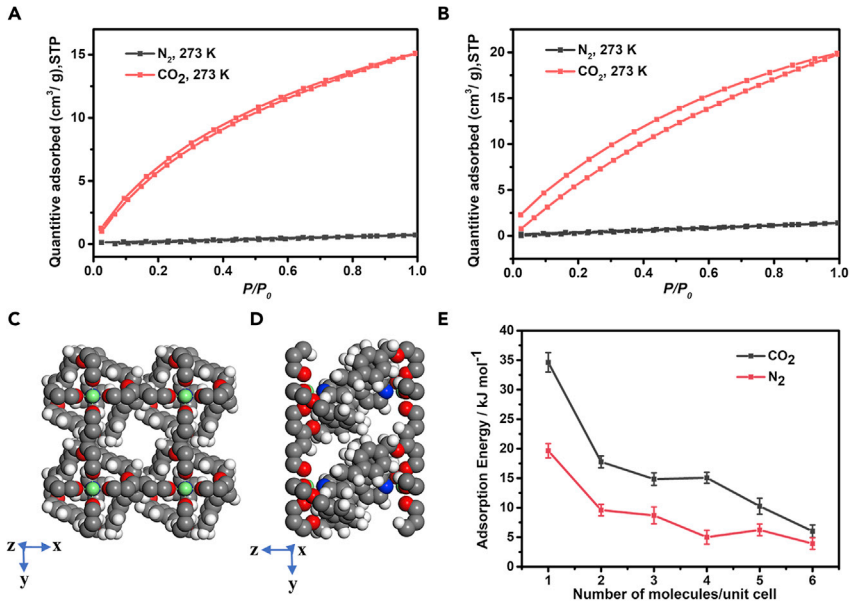

Figure 2. The gas adsorption properties of BUCT MOFs

The adsorption/desorption isotherms of N_2 and CO_2 at 273 K for BUCT-1 (A) and BUCT-2 (B). Top (C) and side (D) views of nano-channel in BUCT-1 MOF (C, gray; H, white; Zn, green; O, red; N, blue). (E) The adsorption energy of MOF nanopores to the individual N_2 or CO_2 molecules with the increase of gas loading amount.

energy of MOF nanopores to the individual N_2 or CO_2 molecules gradually decreased with the increase in gas loading, and the maximum loading was ~6 molecules per unit cell. This result was comparatively in accordance with the experimental adsorption data in Figure 2A; in which, the adsorbed CO_2 molecules was ~3 per unit cell. As expected, BUCT-1 exhibited much higher adsorption energies for CO_2 (6.017 kJ/mol) compared with N_2 (3.921 kJ/mol) indicating its high affinity and selectivity preferring CO_2 over N_2.

Reactivity of BUCT MOFs verified by the thiol-ene click reaction

The purpose of designing BUCT MOFs with polymerizable moieties was to prepare flexible stand-alone MMMs with compatible MOF/polymer interface adhesion and flawless structure. Thus, we first verified the presence of double bonds in MOFs and studied their polymerization ability. BUCT MOFs were digested in 1 mol/L NaOH solution in D_2O and subjected to NMR measurements (Figures S14 and S15). ^{1}H NMR spectra of the decomposed MOFs showed prominent resonances at 5.57 and 5.05 ppm for BUCT-1 and 4.83 and 2.03 ppm for BUCT-2, which were attributed to double bonds. We then demonstrated that the vinyl-containing BUCT MOFs could undergo a "thiol-ene" click reaction with 2-mercaptoethanol. The "clicked" BUCT-1 was digested in 1 mol/L NaOH and tested using ^{1}H NMR. The double bonds of BUCT-1 disappeared and new resonances at 3.36 and 2.76–2.39 ppm appeared corresponding to alkyl chains of organic linkers (Figure S16), indicating the successful occurrence of the thiol-ene click reaction. The S content of clicked BUCT-1 was 4.13 wt% obtained from XPS elemental analysis (Table S6 and Figure S17), which also confirmed the reactivity of double bonds. The PXRD patterns in Figure S18 revealed broad diffraction peaks implying BUCT-1 maintained partial of its crystallinity. In the case of BUCT-2, although the product after "thiol-ene" click reaction could not be digested thoroughly by NaOH, the ^{1}H NMR spectra showed the number of double bonds decreased after the reaction as indicated from the decrease in the integral value of peak 9 (H of double bonds) (Figure S19). We also observed the appearance of new resonances at 3.427-3.409, 2.198, and 0.956 ppm in clicked BUCT-2, confirming the success of the click reaction, and the conversion yield of vinyl groups in BUCT-2 was calculated to be 26.3%. The clicked BUCT-2 revealed 4.98 wt% S in BUCT-2 which exceeded the theoretical value calculated from the conversion yield (Table S6 and Figure S20). This unexpected result might be attributed to the longer side chains in linker 2 causing the cross-linking within BUCT-2 thereafter adsorbing 2-mercaptoethanol on BUCT-2 surface. The loss of crystallinity of BUCT-2 was also presumably owing to the cross-linking of BUCT-2 (Figure S18B).

To further confirm the reactivity of double bonds, BUCT MOFs were also reacted with 1,8-octanedithiol under click conditions. The products were characterized by XPS elemental analysis revealing 7.64 and 7.86 wt % S in each clicked BUCT MOF, respectively (Table S6 and Figures S21 and S22). Moreover, all of the core-level spectrum of S 2p split into spin-orbit doublets of S 2p3/2 and S 2p1/2 (with a typical splitting magnitude of 1.2 eV), and two 2p3/2 peaks were observed ascribing to sulfur of H-S-C (~163.0 eV) and R-S-C (~164.0 eV) (Figures S23 and S24) (Chua and Pumera, 2015). These results confirmed that the C=C bonds in BUCT MOFs could successfully react with the thiol groups via the "thiol-ene" click reaction. The clicked MOFs were then digested using 1 mol/L NaOH in D_2O. Despite the produced solids could not be completely digested, the inductively coupled plasma-mass spectrometry (ICP-MS) analysis revealed the presence of Zn^{2+} in the supernatant (Table S7) implying their partial decomposition. Similarly, the two BUCT MOFs lost their crystallinity after the click reaction with 1,8-octanedithiol (Figure S16). We cannot obtain the ^{1}H NMR spectra of the digested products as they were insoluble in deuterated solvents such as D_2O, $CDCl_3$, DMSO-d_6, and CH_3COOD. Both the loss of crystallinity and the decreased solubility suggested the formation of cross-linked polymer network.

As a control experiment, we also synthesized pillared-layered MOF-508 that featured similar framework structures with BUCT MOFs but without any double bonds. The SEM image in Figure S25 revealed similar morphologies of MOF-508 and BUCT-2. Not surprisingly, MOF-508 without reactive double bonds did not undergo any click reaction as indicated from the ^{1}H NMR spectra of digested products (Figures S26 and S27). The presence of 0.51 at% S in clicked MOF-508 was probably owing to the physical adsorption of 2-mercaptoethanol in MOF-508 (Table S8 and Figure S28). The aforementioned results indicated that the functional C=C double bonds of BUCT MOFs indeed serve as polymerizable groups with high reactivity.

Characterizations of BUCT-MOF-based MMMs

Flexible stand-alone MOF-based MMMs were successfully prepared via copolymerization of BUCT MOFs with poly(ethylene glycol) methyl ether acrylate (PEGMEA) and poly(ethylene glycol) diacrylate (PEGDA). As shown in Figure 3A, the obtained MMMs were flexible and could be curled by hand. Their PXRD patterns in Figure S30A suggested that the crystallinity of BUCT MOFs was well maintained in the MMMs. The TGA plots presented in Figure S30B specified the residual weights representing ZnO were 4.6, 5.1, and 8.7 wt% for MMMs prepared from BUCT-1, BUCT-2, and MOF-508, respectively. Their corresponding MOF loading capacity was 29.0, 31.8 and 31.3 wt%, which was consistent with the initial 30 wt% feeding. The TGA result also confirmed the good thermal stability of the MMMs. The SEM images of MMMs prepared from BUCT MOFs were presented in Figures 3B and Figure S31. Clearly, the BUCT MOFs were well distributed within polymer matrix without any voids at the MOF/polymer interface. The interfacial interaction between BUCT MOFs and polymer matrices was also characterized by FTIR (Figure 3C). Clearly, the two BUCT MOFs and acrylate-terminated monomers (PEGMEA and PEGDA) displayed the prominent peaks centered at 1,610 cm-^{1} (C=C stretching vibration) and 1,420-1,410 cm-^{1} (=CH_2 rocking vibration) (Jiang et al., 2017). These characteristic bands diminished BUCTs-based MMMs implying the polymerization of C=C bonds. For comparison, we also prepared MMM by mixing the as-synthesized MOF-508 (with no double bonds) in the mixture of PEG monomers followed by polymerization. The SEM image in Figure 3B demonstrated that the MOF-508-based MMM featured poor interfacial adhesion with nonselective defects between MOF and polymer interface, which significantly decreased the separation performances of the membranes. These results verified that the introduction of polymerizable double bonds in MOFs greatly enhanced their interfacial interactions with the polymer.

Gas separation performance of BUCT-MOF-based MMMs

Considering the high selectivity of pillared-layered BUCT MOFs toward CO_2 over N_2, the as-prepared MMMs were used for the separation of CO_2 from flue gas. The separation performances were first evaluated using single gas. As seen in Table S9, the plain cross-linked PEO membrane exhibited a CO_2 permeability of 427.7 barrer with a selectivity of 33.4 for CO_2/N_2. After the incorporation of 30 wt% MOF-508 crystals, the resulting MMMs showed a slight increase to 484.7 barrer in CO_2 permeability with a minor decrease in CO_2/N_2 selectivity to 33. The enhanced permeability could be ascribed to the molecular sieving effect of MOF fillers (VandeVondele et al., 2005). By contrast, the MMMs prepared from polymerizable BUCT MOFs with the same loading amount of 30 wt% featured a remarkably enhanced separation performance thanks to the good interfacial compatibility and structures with no defects (Figure 4A). In particular, BUCT-2-based MMMs exhibited the best performance with a CO_2

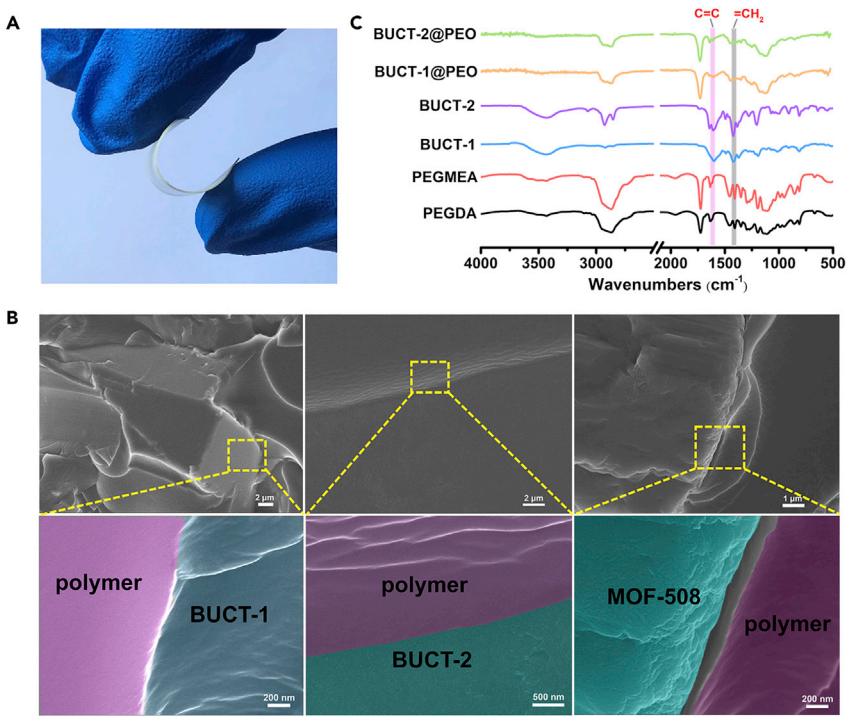

Figure 3. Characterizations of BUCT-MOF-based mixed matrix membranes

(A) Photographs of BUCT-1 based MMMs (the MOF loading amount is 30 wt%).

(B) FTIR spectra of pristine BUCT MOFs, PEG monomers and MOFs based mixed matrix membranes.

(C) Scanning electron microscopy images of cross sections of MOF/polymer MMMs.

permeability of 635.1 barrer and a CO_2/N_2 selectivity of 41.8. These characteristics exceeded the values reported for similar materials elsewhere and almost surpassed the upper-bound limits for polymer-based membranes for CO_2/N_2 separation (Figure 4B and Table S10) (Al-Maythalony et al., 2017; Bae and Long, 2013; Ding et al., 2020; Li et al., 2016; Nafisi and Hägg, 2014; Song et al., 2012; Su et al., 2016; Xin et al., 2015).

We then studied the separation performances of membranes using simulative flue gas containing 0.05% NO_2, 0.10% SO_2, 5.06% O_2, 15.00% CO_2, and 79.79% N_2. Although a slight decrease in permeability and selectivity was observed in all the tested membranes, dramatic 150.6% and 142.1% improvements of CO_2 permeability were obtained in BUCT-2-based MMMs compared with the pristine PEO membrane and MOF-508-based MMMs (Table S9). The relevant CO_2/N_2 selectivity showed 125.4% and 122.3% enhancements in comparison with its counterparts. Notably, no obvious changes were observed in both permeability and selectivity by altering the content of CO_2 in gas mixture or varying the temperature and pressure (Tables S11 and S12). To examine the long-term operational stability of MMMs, we evaluated the gas separation performances of BUCT-2-based MMMs as a function of time. As shown in Table S13, the permeability and selectivity of BUCT-2-based MMMs maintained 504.5 barrer and 35.3 in the separation of simulative flu gas after 5 days. However, a 38% and 29.5% decrease was observed in permeability and selectivity after 10 days, which could be ascribed to the instability of BUCT Zn-MOFs in the moist environment.

Conclusion

We have presented the successful preparation of new pillared-layered polymerizable MOFs by synthesizing benzenedicarboxylic acid linkers containing reactive double bonds attaching to alkyl groups of varying chain lengths. Their crystal structures were elucidated by single-crystal X-ray crystallography. The reactivity of these double bonds was well demonstrated via the efficient thiol-ene click reaction with sulfhydryl compounds. As a result, high affinity and selectivity to CO_2 over other gas molecules such as N_2 was achieved. The MMMs containing covalently linked BUCT MOFs were prepared using copolymerization with poly(ethylene glycol) monomers. These membranes exhibited significantly enhanced separation performances for

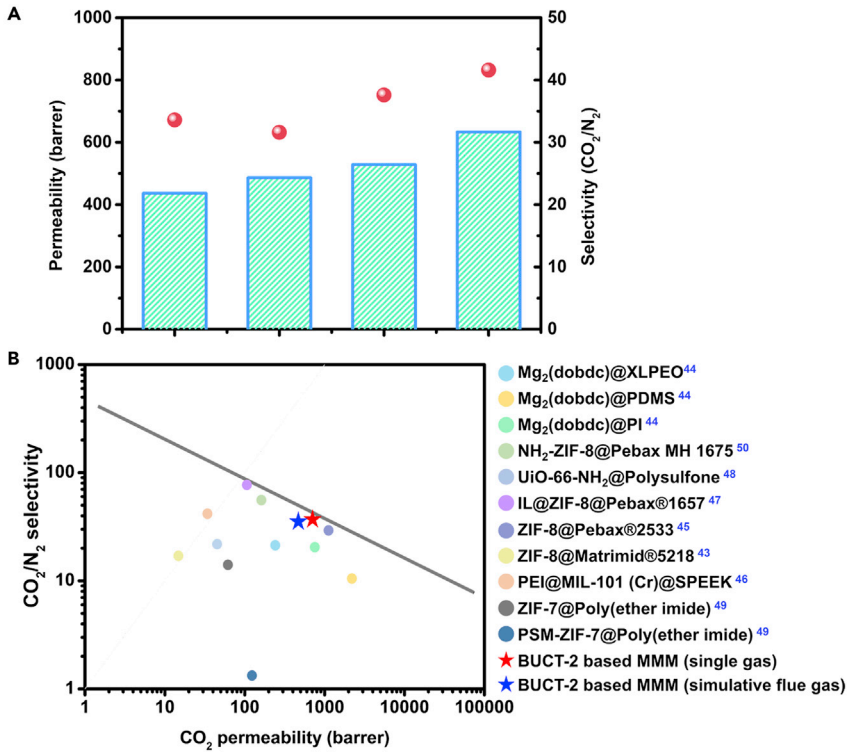

Figure 4. Gas separation performances of BUCT-MOF-based mixed matrix membranes

(A) Comparison of gas separation performances of MMMs prepared from BUCT MOFs, MOF-508, and the pristine polymer membrane.

(B) Gas separation performances of BUCT-2-based MMM in comparison with the state-of-the-art membranes reported in the literature. For exact data, see Table S6. The black line denotes the 2008 upper bound of polymer membranes for CO_2/N_2 separation (Al-Maythalony et al., 2017; Bae and Long, 2013; Ding et al., 2020; Li et al., 2016; Nafisi and Hägg, 2014; Song et al., 2012; Su et al., 2016; Xin et al., 2015).

the separation of CO_2 from simulative flue gas attributing to the improved MOF/polymer interface adhesion. We anticipate that the exploration of new polymerizable BUCT MOFs will open new avenues to the preparation of highly efficient MMMs in various shapes.

Limitations of the study

We have synthesized a class of new pillared-layered polymerizable MOFs containing functional vinyl moieties, which served as a promising platform for the preparation of MOF-based mixed-matrix membranes. The membranes have been tested in the separation of flue gas under different various conditions; however, other gas mixtures such as biogas have not been studied. Our continuing work will focus on testing more gas mixtures and evaluate the applicability of membranes in practical applications.

STAR★METHODS

Detailed methods are provided in the online version of this paper and include the following:

- KEY RESOURCES TABLE
- RESOURCE AVAILABILITY
  - Lead contact
  - Materials availability
  - Data and code availability
- METHOD DETAILS
  - Materials and regents
  - Instrumentation

- Synthesis of 2,5-dihydroxy-1,4-benzenedicarboxylate
- Synthesis of 2,5-bis((4-vinylbenzyl)oxy)-1,4-benzenedicarboxylic acid (linker 1)
- Synthesis of 2,5-bis(oct-7-en-1-yloxy)-1,4-benzenedicarboxylic acid (linker 2)
- Synthesis of BUCT MOFs
- General method of the thiol-ene click reaction
- Preparation of cross-linked PEO membranes containing MOF
- Gas transport measurement
- Computational methods

SUPPLEMENTAL INFORMATION

Supplemental information can be found online at https://doi.org/10.1016/j.isci.2021.102560.

ACKNOWLEDGMENTS

The authors gratefully acknowledge the financial supports from the National Key R & D Program of China (2018YFA0902200), National Natural Science Foundation of China (31961133004, 21861132017), and the Fundamental Research Funds for the Central Universities (PT1917, buctrc201). FS acknowledges support of EFSA-CDN project (No. CZ.02.1.01/0.0/0.0/16_019/0000841) co-funded by ERDF. Work at the Molecular Foundry and Advanced Light Source was supported by the Office of Science, Office of Basic Energy Sciences, of the U.S. Department of Energy under Contract No. DE-AC02-05CH11231.

AUTHOR CONTRIBUTIONS

Y.L. conceived and designed the experiments; Z.C. and D.Y. synthesized the BUCT MOFs and characterized their properties; Z.C. performed the "thiol-ene" click reaction of BUCT MOFs; L.M. and Y.Z. prepared the mixed-matrix membranes and measured their gas separation performances; J.Z. and H.L. performed the DFT simulation; R.K. and J.Z. tested and refined the crystal structures; F.S. and T.T. directed the projects. Y.L. and Z.C. wrote the manuscript, and all authors contributed to revising the paper.

DECLARATION OF INTERESTS

The authors declare no competing interests.

Received: March 25, 2021
Revised: May 10, 2021
Accepted: May 14, 2021
Published: June 25, 2021

REFERENCES

Al-Maythalony, B.A., Alloush, A.M., Faizan, M., Dafallah, H., Elgzoly, M.A.A., Seliman, A.A.A., Al-Ahmed, A., Yamani, Z.H., Habib, M.A.M., Cordova, K.E., and Yaghi, O.M. (2017). Tuning the interplay between selectivity and permeability of ZIF-7 mixed matrix membranes. ACS Appl. Mater. Interfaces *9*, 33401–33407.

Albalad, J., Xu, H., Gándara, F., Haouas, M., Martineau-Corcos, C., Mas-Ballesté, R., Barnett, S.A., Juanhuix, J., Imaz, I., and Maspoch, D. (2018). Single-Crystal-to-Single-Crystal postsynthetic modification of a metal–organic framework via ozonolysis. J. Am. Chem. Soc. *140*, 2028–2031.

Bae, T.-H., and Long, J.R. (2013). CO2/N2 separations with mixed-matrix membranes containing Mg2(dobdc) nanocrystals. Energy Environ. Sci. *6*, 3565–3569.

Baker, R.W., and Low, B.T. (2014). Gas separation membrane materials: a perspective. Macromolecules *47*, 6999–7013.

Bastani, D., Esmaeili, N., and Asadollahi, M. (2013). Polymeric mixed matrix membranes containing zeolites as a filler for gas separation applications: a review. J. Ind. Eng. Chem. *19*, 375–393.

Bernardo, P., Drioli, E., and Golemme, G. (2009). Membrane gas separation: a review/state of the art. Ind. Eng. Chem. Res. *48*, 4638–4663.

Brunetti, A., Scura, F., Barbieri, G., and Drioli, E. (2010). Membrane technologies for CO2 separation. J. Membr. Sci. *359*, 115–125.

Chang, Y., Huang, H., Wang, L., Li, Y., and Zhong, C. (2020). Synergistic dual-Li+ sites for CO2 separation in metal-organic framework composites. Chem. Eng. J. *402*, 126201.

Chua, C.K., and Pumera, M. (2015). Monothiolation and reduction of graphene oxide via one-pot synthesis: hybrid catalyst for oxygen reduction. ACS Nano *9*, 4193–4199.

Cohen, S.M. (2012). Postsynthetic methods for the functionalization of metal–organic frameworks. Chem. Rev. *112*, 970–1000.

Cohen, S.M. (2017). The postsynthetic renaissance in porous solids. J. Am. Chem. Soc. *139*, 2855–2863.

D'Alessandro, D.M., Smit, B., and Long, J.R. (2010). Carbon dioxide capture: prospects for new materials. Angew. Chem. Int. Ed. *49*, 6058–6082.

Dechnik, J., Gascon, J., Doonan, C.J., Janiak, C., and Sumby, C.J. (2017). Mixed-matrix membranes. Angew. Chem. Int. Ed. *56*, 9292–9310.

Deng, Y., Wu, Y., Chen, G., Zheng, X., Dai, M., and Peng, C. (2021). Metal-organic framework membranes: recent development in the synthesis strategies and their application in oil-water separation. Chem. Eng. J. *405*, 127004.

Denny, M.S., Moreton, J.C., Benz, L., and Cohen, S.M. (2016). Metal–organic frameworks for

membrane-based separations. Nat. Rev. Mater. *1*, 16078.

Ding, R., Zheng, W., Yang, K., Dai, Y., Ruan, X., Yan, X., and He, G. (2020). Amino-functional ZIF-8 nanocrystals by microemulsion based mixed linker strategy and the enhanced CO2/N2 separation. Sep. Purif. Technol. *236*, 116209.

Dong, G., Li, H., and Chen, V. (2013). Challenges and opportunities for mixed-matrix membranes for gas separation. J. Mater. Chem. A. *1*, 4610–4630.

Elsaidi, S.K., Venna, S., Sekizkardes, A.K., Steckel, J.A., Mohamed, M.H., Baker, J., Baltrus, J., and Hopkinson, D. (2020). Custom formulation of multicomponent mixed-matrix membranes for efficient post-combustion carbon capture. Cell Rep. Phys. Sci. *1*, 100113.

Feijani, E.A., Mahdavi, H., and Tavasoli, A. (2015). Poly(vinylidene fluoride) based mixed matrix membranes comprising metal organic frameworks for gas separation applications. Chem. Eng. Res. Des. *96*, 87–102.

Furukawa, H., Cordova, K.E., O'Keeffe, M., and Yaghi, O.M. (2013). The chemistry and applications of metal-organic frameworks. Science *341*, 1230444.

Garzón-Tovar, L., Rodríguez-Hermida, S., Imaz, I., and Maspoch, D. (2017). Spray drying for making covalent chemistry: postsynthetic modification of metal–organic frameworks. J. Am. Chem. Soc. *139*, 897–903.

Goedecker, S., Teter, M., and Hutter, J. (1996). Separable dual-space Gaussian pseudopotentials. Phys. Rev. B *54*, 1703–1710.

Goh, P.S., Ismail, A.F., Sanip, S.M., Ng, B.C., and Aziz, M. (2011). Recent advances of inorganic fillers in mixed matrix membrane for gas separation. Sep. Purif. Technol. *81*, 243–264.

Grimme, S., Antony, J., Ehrlich, S., and Krieg, H. (2010). A consistent and accurate ab initio parametrization of density functional dispersion correction (DFT-D) for the 94 elements H-Pu. J. Chem. Phys. *132*, 154104.

Guo, X., Qiao, Z., Liu, D., and Zhong, C. (2019). Mixed-matrix membranes for CO2 separation: role of the third component. J. Mater. Chem. A *7*, 24738–24759.

Guo, Z., Liu, Z., Zhang, K., Wang, W., Pang, J., Li, Z., Kang, Z., and Zhao, D. (2021). Stable metal-organic frameworks based mixed matrix membranes for Ethylbenzene/N2 separation. Chem. Eng. J. *416*, 129193.

Henke, S., and Fischer, R.A. (2011). Gated channels in a honeycomb-like Zinc−Dicarboxylate−Bipyridine framework with flexible alkyl ether side chains. J. Am. Chem. Soc. *133*, 2064–2067.

Henke, S., Schmid, R., Grunwaldt, J.-D., and Fischer, R.A. (2010). Flexibility and sorption selectivity in rigid metal–organic frameworks: the impact of ether-functionalised linkers. Chem. A Eur. J. *16*, 14296–14306.

Henke, S., Schneemann, A., Wütscher, A., and Fischer, R.A. (2012). Directing the breathing behavior of pillared-layered metal–organic frameworks via a systematic library of functionalized linkers bearing flexible substituents. J. Am. Chem. Soc. *134*, 9464–9474.

Hou, L., Wang, L., Zhang, N., Xie, Z., and Dong, D. (2016). Polymer brushes on metal–organic frameworks by UV-induced photopolymerization. Polym. Chem. *7*, 5828–5834.

Javaid, A. (2005). Membranes for solubility-based gas separation applications. Chem. Eng. J. *112*, 219–226.

Jiang, W.-L., Ding, L.-G., Yao, B.-J., Wang, J.-C., Chen, G.-J., Li, Y.-A., Ma, J.-P., Ji, J., Dong, Y., and Dong, Y.-B. (2016). A MOF-membrane based on the covalent bonding driven assembly of a NMOF with an organic oligomer and its application in membrane reactors. Chem. Commun. *52*, 13564–13567.

Jiang, X., Li, S., and Shao, L. (2017). Pushing CO2-philic membrane performance to the limit by designing semi-interpenetrating networks (SIPN) for sustainable CO2 separations. Energy Environ. Sci. *10*, 1339–1344.

Kertik, A., Wee, L.H., Pfannmöller, M., Bals, S., Martens, J.A., and Vankelecom, I.F.J. (2017). Highly selective gas separation membrane using in situ amorphised metal–organic frameworks. Energy Environ. Sci. *10*, 2342–2351.

Krack, M. (2005). Pseudopotentials for H to Kr optimized for gradient-corrected exchange-correlation functionals. Theor. Chem. Acc. *114*, 145–152.

Kühne, T.D., Iannuzzi, M., Del Ben, M., Rybkin, V.V., Seewald, P., Stein, F., Laino, T., Khaliullin, R.Z., Schütt, O., Schiffmann, F., et al. (2020). CP2K: an electronic structure and molecular dynamics software package - quickstep: Efficient and accurate electronic structure calculations. J. Chem. Phys. *152*, 194103.

Li, H., Eddaoudi, M., O'Keeffe, M., and Yaghi, O.M. (1999). Design and synthesis of an exceptionally stable and highly porous metal-organic framework. Nature *402*, 276–279.

Li, H., Tuo, L., Yang, K., Jeong, H.-K., Dai, Y., He, G., and Zhao, W. (2016). Simultaneous enhancement of mechanical properties and CO2 selectivity of ZIF-8 mixed matrix membranes: interfacial toughening effect of ionic liquid. J. Membr. Sci. *511*, 130–142.

Lin, R., Villacorta Hernandez, B., Ge, L., and Zhu, Z. (2018). Metal organic framework based mixed matrix membranes: an overview on filler/polymer interfaces. J. Mater. Chem. A *6*, 293–312.

Ma, L., Svec, F., Lv, Y., and Tan, T. (2019a). Engineering of the filler/polymer interface in metal–organic framework-based mixed-matrix membranes to enhance gas separation. Chem. Asian J. *14*, 3502–3514.

Ma, L., Svec, F., Lv, Y., and Tan, T. (2019b). In situ bottom–up growth of metal–organic frameworks in a crosslinked poly(ethylene oxide) layer with ultrahigh loading and superior uniform distribution. J. Mater. Chem. A *7*, 20293–20301.

Molavi, H., Shojaei, A., and Mousavi, S.A. (2018). Improving mixed-matrix membrane performance via PMMA grafting from functionalized NH2–UiO-66. J. Mater. Chem. A *6*, 2775–2791.

Moore, T.T., and Koros, W.J. (2005). Non-ideal effects in organic–inorganic materials for gas separation membranes. J. Mol. Struct. *739*, 87–98.

Morris, W., Doonan, C.J., Furukawa, H., Banerjee, R., and Yaghi, O.M. (2008). Crystals as molecules: postsynthesis covalent functionalization of zeolitic imidazolate frameworks. J. Am. Chem. Soc. *130*, 12626–12627.

Nafisi, V., and Hägg, M.-B. (2014). Development of dual layer of ZIF-8/PEBAX-2533 mixed matrix membrane for CO2 capture. J. Membr. Sci. *459*, 244–255.

Park, H.B., Kamcev, J., Robeson, L.M., Elimelech, M., and Freeman, B.D. (2017). Maximizing the right stuff: the trade-off between membrane permeability and selectivity. Science *356*, eaab0530.

Perdew, J.P., Burke, K., and Ernzerhof, M. (1996). Generalized gradient approximation made simple. Phys. Rev. Lett. *77*, 3865–3868.

Prasetya, N., Himma, N.F., Sutrisna, P.D., Wenten, I.G., and Ladewig, B.P. (2020). A review on emerging organic-containing microporous material membranes for carbon capture and separation. Chem. Eng. J. *391*, 123575.

Rezakazemi, M., Ebadi Amooghin, A., Montazer-Rahmati, M.M., Ismail, A.F., and Matsuura, T. (2014). State-of-the-art membrane based CO2 separation using mixed matrix membranes (MMMs): an overview on current status and future directions. Prog. Polym. Sci. *39*, 817–861.

Seoane, B., Coronas, J., Gascon, I., Benavides, M.E., Karvan, O., Caro, J., Kapteijn, F., and Gascon, J. (2015). Metal–organic framework based mixed matrix membranes: a solution for highly efficient CO2 capture? Chem. Soc. Rev. *44*, 2421–2454.

Shahid, S., Nijmeijer, K., Nehache, S., Vankelecom, I., Deratani, A., and Quemener, D. (2015). MOF-mixed matrix membranes: precise dispersion of MOF particles with better compatibility via a particle fusion approach for enhanced gas separation properties. J. Membr. Sci. *492*, 21–31.

Song, Q., Nataraj, S.K., Roussenova, M.V., Tan, J.C., Hughes, D.J., Li, W., Bourgoin, P., Alam, M.A., Cheetham, A.K., Al-Muhtaseb, S.A., and Sivaniah, E. (2012). Zeolitic imidazolate framework (ZIF-8) based polymer nanocomposite membranes for gas separation. Energy Environ. Sci. *5*, 8359–8369.

Su, N.C., Sun, D.T., Beavers, C.M., Britt, D.K., Queen, W.L., and Urban, J.J. (2016). Enhanced permeation arising from dual transport pathways in hybrid polymer–MOF membranes. Energy Environ. Sci. *9*, 922–931.

Tien-Binh, N., Vinh-Thang, H., Chen, X.Y., Rodrigue, D., and Kaliaguine, S. (2015). Polymer functionalization to enhance interface quality of mixed matrix membranes for high CO2/CH4 gas separation. J. Mater. Chem. A *3*, 15202–15213.

VandeVondele, J., and Hutter, J. (2007). Gaussian basis sets for accurate calculations on molecular

systems in gas and condensed phases. J. Chem. Phys. *127*, 114105.

VandeVondele, J., Krack, M., Mohamed, F., Parrinello, M., Chassaing, T., and Hutter, J. (2005). Quickstep: fast and accurate density functional calculations using a mixed Gaussian and plane waves approach. Comput. Phys. Commun. *167*, 103–128.

Venna, S.R., Lartey, M., Li, T., Spore, A., Kumar, S., Nulwala, H.B., Luebke, D.R., Rosi, N.L., and Albenze, E. (2015). Fabrication of MMMs with improved gas separation properties using externally-functionalized MOF particles. J. Mater. Chem. A *3*, 5014–5022.

Wang, H., He, S., Qin, X., Li, C., and Li, T. (2018). Interfacial engineering in metal–organic framework-based mixed matrix membranes using covalently grafted polyimide brushes. J. Am. Chem. Soc. *140*, 17203–17210.

Wang, S., Li, X., Wu, H., Tian, Z., Xin, Q., He, G., Peng, D., Chen, S., Yin, Y., Jiang, Z., and Guiver, M.D. (2016). Advances in high permeability polymer-based membrane materials for CO2 separations. Energy Environ. Sci. *9*, 1863–1890.

Xin, Q., Ouyang, J., Liu, T., Li, Z., Li, Z., Liu, Y., Wang, S., Wu, H., Jiang, Z., and Cao, X. (2015). Enhanced interfacial interaction and CO2 separation performance of mixed matrix membrane by incorporating polyethylenimine-decorated metal–organic frameworks. ACS Appl. Mater. Interfaces *7*, 1065–1077.

Yin, Z., Wan, S., Yang, J., Kurmoo, M., and Zeng, M.-H. (2019). Recent advances in post-synthetic modification of metal–organic frameworks: new types and tandem reactions. Coord. Chem. Rev. *378*, 500–512.

Yoo, D.K., Yoon, T.-U., Bae, Y.-S., and Jhung, S.H. (2020). Metal-organic framework MIL-101 loaded with polymethacrylamide with or without further reduction: effective and selective CO2 adsorption with amino or amide functionality. Chem. Eng. J. *380*, 122496.

Yu, J., Xie, L.-H., Li, J.-R., Ma, Y., Seminario, J.M., and Balbuena, P.B. (2017). CO2 capture and separations using MOFs: computational and experimental studies. Chem. Rev. *117*, 9674–9754.

Zhang, Y., Feng, X., Li, H., Chen, Y., Zhao, J., Wang, S., Wang, L., and Wang, B. (2015). Photoinduced postsynthetic polymerization of a metal–organic framework toward a flexible stand-alone membrane. Angew. Chem. Int. Ed. *54*, 4259–4263.

Zhou, H.-C.J., and Kitagawa, S. (2014). Metal–organic frameworks (MOFs). Chem. Soc. Rev. *43*, 5415–5418.

STAR★METHODS

KEY RESOURCES TABLE

REAGENT or RESOURCE	SOURCE	IDENTIFIER
Chemicals, Peptides, and Recombinant Proteins		
Zinc nitrate hexahydrate	J&K Scientific Ltd (Beijing, China)	CAS: 10196-18-6
4,4′-bipyridine	J&K Scientific Ltd (Beijing, China)	CAS: 553-26-4
methyl ether acrylate (M_n, 480 g/mol)	J&K Scientific Ltd (Beijing, China)	CAS: 32171-39-4
poly(ethylene glycol) diacrylate (M_n, 700 g/mol)	J&K Scientific Ltd (Beijing, China)	CAS: 26570-48-9
2,5-Dihydroxy-1,4-benzenedicarboxylic acid	Sigma-Aldrich (St. Louis, USA)	CAS: 610-92-4
4-Vinylbenzyl chloride	Macklin (Shanghai, China)	CAS: 1592-20-7
2,2′-azobis(2-methylpropionitrile) (AIBN)	Macklin (Shanghai, China)	CAS: 78-67-1
2-mercaptoethanol	Macklin (Shanghai, China)	CAS: 60-24-2
8-bromo-1-octene	Heowns (Tianjin, China)	CAS: 2695-48-9
1,8-octanedithiol	Adamas-beta (Shanghai, China)	CAS: 1191-62-4
Deposited data		
BUCT-1 crystal structure	This paper	CCDC number: 2053658
BUCT-2 crystal structure	This paper	CCDC number: 2052358
Software and algorithms		
CP2K package	(Kühne et al., 2020; VandeVondele et al., 2005)	https://doi.org/10.1063/5.0007045

RESOURCE AVAILABILITY

Lead contact

Further information and requests for resources and reagents should be directed to and will be fulfilled by the lead contact, Yongqin Lv (lvyq@mail.buct.edu.cn).

Materials availability

This study did not generate new unique reagents.

Data and code availability

The crystal data of BUCT-1 and BUCT-2 generated during this study were deposited into the Cambridge Crystallographic Data Centre (CCDC) and assigned numbers 2053658 and 2052358, respectively.

METHOD DETAILS

Materials and regents

Zinc nitrate hexahydrate, 4,4′-bipyridine, poly(ethylene glycol) methyl ether acrylate (Mn, 480 g/mol), and poly(ethylene glycol) diacrylate (Mn, 700 g/mol) were purchased from J&K Scientific Ltd (Beijing, China). 2,5-Dihydroxy-1,4-benzenedicarboxylic acid was obtained from Sigma-Aldrich (St. Louis, USA). 4-Vinylbenzyl chloride, 2,2′-azobis(2-methylpropionitrile) (AIBN), and 2-mercaptoethanol were received from Macklin (Shanghai, China), 8-bromo-1-octene was purchased from Heowns (Tianjin, China), and 1,8-octanedithiol was provided by Adamas-beta (Shanghai, China). All other reagents were bought from Sinopharm Chemical Reagent Co., Ltd (Beijing, China) and Beijing Chemical Works (Beijing, China).

Instrumentation

Scanning electron microscopy images of BUCT MOFs and MOF-polymer composites were obtained from a JEOL JSM-7610F field emission scanning electron microscope (Hitachi High-Technologies, Tokyo, Japan). Elemental analysis of BUCT MOFs was performed using an energy-dispersive X-ray spectrometer Quantax 200 XF 5010 (Bruker, Germany). Powder X-ray diffraction patterns of BUCT MOFs, MOF-508, and MOF-polymer composites were collected using a Bruker D8 Advance (Bruker Corporation, Germany). X-ray

photoelectron spectroscopy measurements of clicked MOFs were carried out using an EscaLab 250Xi (Thermo Fisher Scientific, America). High-pressure CO_2 and N_2 sorption measurements were performed on an HSorb2600 high pressure and temperature gas sorption analyzer (Gold APP Instruments Corporation, Beijing, China). Thermogravimetric analysis of BUCT MOFs and MOF-polymer composites was carried out under an air atmosphere using a DTG-60A (Shimadzu, Japan) at a heating rate of 10°C/min ranging from 25 to 800°C. The ^1H and ^{13}C nuclear magnetic resonance (NMR) spectra of organic linkers and digested MOFs were recorded on a 400-MHz Bruker AVANCE III (Bruker Corporation, Germany). The electrospray ionization mass spectrometry measurements of organic linkers were performed using the Xevo G2 QTof mass spectrometer (Waters Corporation, USA). The concentration of Zn^{2+} in the supernatant after the digestion of MOFs was measured using an Agilent 7500CE ICP-MS. FTIR spectra were collected on a Spectrum One FTIR spectrometer (Perkin Elmer, USA). A suitable single crystal of BUCT-1 was selected, and diffraction data were collected on an Agilent Xcalibur (Eos, Gemini) diffractometer using Mo Kα (λ = 0.71073 Å) radiation. The single crystal of BUCT-2 was selected, and diffraction data were collected on beamline 11.3.1 at the Advanced Light Source with λ = 0.7749 Å at 100 K using an Oxford Cryosystems Cryostream 700 plus. The data reduction was corrected for absorption effects using SADABS v2016/2. All structures were solved using SHELXT using the direct method and were refined by least-square refinement against F2 by SHELXL. The crystal data file of BUCT-1 and BUCT-2 was deposited into the Cambridge Crystallographic Data Centre (CCDC) and assigned numbers 2053658 and 2052358, respectively.

Synthesis of 2,5-dihydroxy-1,4-benzenedicarboxylate

2,5-Dihydroxy-1,4-benzenedicarboxylic acid (5 g, 25.2 mmol) was first esterified in dry methanol using SOCl2 (11 g, 0.1 mol) as the catalyst. The mixture was refluxed at 70°C for 8 h. After the reaction was completed, the yellow product was obtained by removing the solvent via evaporation, dissolving in dichloromethane, and further extracting using saturated NaHCO3 aqueous solution, saturated NaCl solution, and water. The final yellow powder of 2,5-dihydroxy-1,4-benzenedicarboxylate was obtained after drying under vacuum (4.8 g, 84.2% yield). ^1H NMR (400 MHz, $CDCl_3$, 298 K, ppm): δ 9.97 (s, 2H, OH), 7.38 (s, 2H, Ar—H), 3.89 (s, 6H, CH_3); ^{13}C NMR (400 MHz, $CDCl_3$, 298 K, ppm): 169.47, 152.91, 118.32, 117.76, 52.78.

Synthesis of 2,5-bis((4-vinylbenzyl)oxy)-1,4-benzenedicarboxylic acid (linker 1)

The 2,5-dihydroxy-1,4-benzenedicarboxylate (2 g, 8.84 mmol) was dissolved in *N*, *N*′-dimethylformamide. Vinylbenzyl chloride (2.834 g, 18.57 mmol) and K_2CO_3 (5.491 g, 39.79 mmol) were added into the solution. The mixture was left to react for 12 h at 85°C. After removing the solvent by evaporation, the residue was refluxed at 80°C for 6 h using the mixture of methanol (80 mL) and H_2O (20 mL) containing 20.1 mmol NaOH. After cooling to room temperature, methanol was removed, and the mixture left was transferred in 100 mL water. The solution was acidified to pH 6.5 with 1 mol/L HCl. The final white solid product 2,5-bis((4-vinylbenzyl)oxy)-1,4-benzenedicarboxylic acid was obtained by washing with water and dried under vacuum at 85°C (2.88 g, 75.7% yield). ^1H NMR (400 MHz, DMSO-d_6, 298K, ppm): δ 13.07 (s, 2H, OH), 7.42-7.51 (m, 12H, Ar—H), 6.75 (m, 2H, CH), 5.86 (d, 2H, CH_2), 5.44 (d, 2H, CH_2), 5.17 (s, 4H, OCH_2) ppm; ^{13}C NMR (400 MHz, DMSO-d_6, 298K, ppm): δ 166.69, 150.22, 136.64, 136.53, 136.30, 127.44, 126.09, 125.66, 116.09, 114.35, 70.22.

Synthesis of 2,5-bis(oct-7-en-1-yloxy)-1,4-benzenedicarboxylic acid (linker 2)

The 2,5-dihydroxy-1,4-benzenedicarboxylate (1 g, 4.42 mmol) was dissolved in N,N′-dimethylformamide. 8-Bromo-1-octene (1.774 g, 9.28 mmol) and K_2CO_3 (2.746 g, 19.90 mmol) were added to the solution. The mixture reacted for 12 h at 85°C. After removing the solvent by evaporation, the residue was refluxed at 80°C for 6 h using the mixture of methanol (80 mL) and H_2O (20 mL) containing 9.28 mmol NaOH. After cooling to room temperature, methanol was removed and the mixture was transferred to 100 mL water. The solution was acidified to pH 6.5 with 1 mol/L HCl. The final white solid product 2,5-bis(oct-7-en-1-yloxy)-1,4-benzenedicarboxylic acid was obtained by washing with water and dried under vacuum at 85°C (1.337 g, 72.3% yield). ^1H NMR (400 MHz, DMSO-d_6, 298K, ppm): δ 12.94 (s, 2H, OH), 7.21 (s, 2H, Ar—H), 5.81 (m, 2H, CH), 4.98 (m, 4H, CH_2), 3.96 (m, 4H, CH_2), 2.03 (m, 4H, CH_2), 1.67 (m, 4H, CH_2), 1.44-1.31 (m, 12H, CH_2); ^{13}C NMR (400 MHz, DMSO-d_6, 298K, ppm): δ 166.96, 150.37, 138.78, 125.90, 115.47, 114.61, 69.10, 33.07, 28.64, 28.21, 25.12.

Synthesis of BUCT MOFs

For the synthesis of BUCT MOFs, $Zn(NO_3)_2 \cdot 6H_2O$ (1.16 mmol), 4,4′-bipyridine (1.16 mmol), and linker (1.16 mmol) were dissolved in the solvent mixture containing 80 mL DMF and 4 mL ethanol. This mixture was reacted in a 100-mL autoclave at 85°C for 48 h. The resulting solid was first washed with DMF (5 × 8 mL) and then with ethanol (3 × 8 mL), further activated via immersing the crystals in CH_2Cl_2 for 8 h and dried under vacuum at 120°C overnight to produce the yellow BUCT-1.

General method of the thiol-ene click reaction

For the thiol-ene click reaction, 2-mercaptoethanol or 1,8-octanedithiol (0.176 mmol) was added to a suspension of BUCT MOFs (0.044 mmol) in 200 μL DMF. Then, AIBN (1 wt%) was added to the solution and the mixture was stirred at 70°C for 1 h. The final product was obtained by centrifugation, washed with DMF (3 × 1 mL) and ethanol (5 × 1 mL), and dried under vacuum at 80°C overnight.

Preparation of cross-linked PEO membranes containing MOF

For the preparation of cross-linked PEO membranes containing MOF, BUCT MOFs and MOF-508 particles were added into a mixture of 350 mg poly(ethylene glycol) methyl ether acrylate (Mn, 480 g/mol), 150 mg poly(ethylene glycol) diacrylate (Mn, 700 g/mol), and azobisisobutyronitrile (1 wt% with respect to monomers). The weight loading of BUCTs and MOF-508 particles was 30 wt%. The mixture was homogenized by sonication for 3 min, degassed by purging with nitrogen for 5 min, and then filled into a mold made up of two glass plates champed together and separated with two Teflon strips with a thickness of 70 μm. The thermally initiated polymerization reaction was carried out in an oven at 65°C for 2 h, and the mold was incubated in water for 30 min to detach the membrane from the glass plates. Finally, the membranes were washed with ethanol and dried at 85°C for 1 h.

Gas transport measurement

Gas separation performance of membranes was determined using method reported previously (Ma et al., 2019a, 2019b). The gas permeation parameters were measured using single gases (CO_2 and CH_4) at 0.5 MPa pressure difference and 35°C.

Computational methods

The first principle calculations were carried out within the framework of density function theory using the QUICKSTEP module in the CP2K package (Kühne et al., 2020; VandeVondele et al., 2005). The Perdew-Burke-Ernzerhof (Perdew et al., 1996) exchange-correlation function was used combined with the Goedecker-Teter-Hutter (Goedecker et al., 1996; Krack, 2005) pseudopotential and the Gaussian and Planar Wave hybrid basis set (VandeVondele and Hutter, 2007). The Grimme semiempirical dispersive correction (Grimme et al., 2010) was also included in the calculation to fully capture the long-range dispersion interaction between MOF and gas molecules. The crystal and adsorption structures were fully relaxed until the maximum atomic force was less than 2.057E-2 eV/Å.